Title

Predictive Model of Charge Mobilities in Organic Semiconductor Small Molecules with Force-Matched Potentials.

Journal

Journal of Chemical Theory and Computation, 16(6)

ISSN

1549-9618

Authors

Dantanarayana, Varuni
Nematiaram, Tahereh
Vong, Daniel
et al.

Publication Date

2020-06-09

DOI

10.1021/acs.jctc.0c00211

Peer reviewed

JCTC Journal of Chemical Theory and Computation

pubs.acs.org/JCTC Article

Predictive Model of Charge Mobilities in Organic Semiconductor Small Molecules with Force-Matched Potentials

Varuni Dantanarayana, Tahereh Nematiaram, Daniel Vong, John E. Anthony, Alessandro Troisi, Kien Nguyen Cong, Nir Goldman, Roland Faller, and Adam J. Moulé*

Cite This: J. Chem. Theory Comput. 2020, 16, 3494–3503 Read Online

ACCESS | Metrics & More | Article Recommendations | Supporting Information

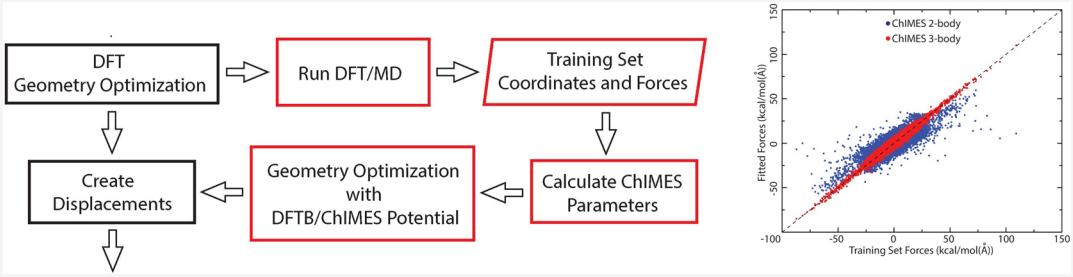

ABSTRACT: Charge mobility of crystalline organic semiconductors (OSC) is limited by local dynamic disorder. Recently, the charge mobility for several high mobility OSCs, including TIPS-pentacene, were accurately predicted from a density functional theory (DFT) simulation constrained by the crystal structure and the inelastic neutron scattering spectrum, which provide direct measures of the structure and the dynamic disorder in the length scale and energy range of interest. However, the computational expense required for calculating all of the atomic and molecular forces is prohibitive. Here we demonstrate the use of density functional tight binding (DFTB), a semiempirical quantum mechanical method that is 2 to 3 orders of magnitude more efficient than DFT. We show that force matching a many-body interaction potential to DFT derived forces yields highly accurate DFTB models capable of reproducing the low-frequency intricacies of experimental inelastic neutron scattering (INS) spectra and accurately predicting charge mobility. We subsequently predicted charge mobilities from our DFTB model of a number of previously unstudied structural analogues to TIPS-pentacene using dynamic disorder from DFTB and transient localization theory. The approach we establish here could provide a truly rapid simulation pathway for accurate materials properties prediction, in our vision applied to new OSCs with tailored properties.

INTRODUCTION

Organic semiconductors (OSCs) are a class of materials that have been at the forefront of new optoelectronic devices, including organic photovoltaic cells (OPV), organic field-effect transistors (OFET), organic light-emitting diodes (OLEDs), biosensors, and nanoscale molecular electronics.[1−6] OSCs are advantageous because they are lightweight, biodegradable, and strong but flexible (wearable) with mechanical properties similar to plastics. Furthermore, devices can be fabricated easily and at low cost over large areas via high-throughput solution deposition techniques such as inkjet printing and roll-to-roll printing,[7] which are more ecologically friendly and more economical than typical inorganic semiconductor fabrication methods.[8−10] Charge mobility (μ) is one of the most important performance metrics used to assess OSCs. Rubrene, the highest mobility OSC to date, has a hole mobility (μ_h) of ∼20−25 cm^2 V^{-1} s^{-1},[11,12] which exceeds the performance of amorphous silicon of ∼10 cm^2 V^{-1} s^{-1}. However, commercialization of OSCs is limited to particular applications because polycrystalline silicon still has a much higher μ_h of ∼400 cm^2 V^{-1} s^{-1}.[1,13,14]

Novel OSC materials with higher μ are in great demand. For OSC materials discovery and optimization, it is imperative to have a thorough understanding of the factors that affect μ, where molecular packing, domain size, and film morphology have been the main targets so far.[15,16] OSCs generally have large molecular masses and are held together by weak van der Waals forces, which means that thermally activated molecular motions can be significant, even under ambient conditions in crystals, in particular, low-frequency and long-time-scale phonons that represent large collective intermolecular motions with vibrational periods of picoseconds to nanoseconds. They

Received: March 3, 2020
Published: May 13, 2020

https://dx.doi.org/10.1021/acs.jctc.0c00211
J. Chem. Theory Comput. 2020, 16, 3494−3503

change on a time scale similar to the charge hopping rate in OSCs. Their effect is to continuously change the instantaneous ground state potential energy surface. Such instantaneous distortions of the equilibrium geometry impact local and nonlocal electronic couplings which in turn affect μ.[17] The collective effect that phonon motions have on the variation of the ground state potential energy surface is known as "dynamic disorder". There is a growing body of evidence that high values of dynamic disorder reduce μ and thereby the performance of OSC materials used in potential applications.[18,19]

Improved synthesis and crystallization techniques have yielded huge advances in OSC materials and performance. The combined knowledge of many experiments leads to the development of empirical design rules that give synthetic chemists new target molecule ideas, but too often the empirical design rule is inaccurate. Recently, it was proposed that the dynamic disorder limits μ_h in OSCs and that μ_h could be predicted with full knowledge of the dynamics.[20,21] Computer simulations can, in principle, provide a much cheaper and faster method to elucidate and visualize molecular level phenomena and material structure/property relationships and can significantly reduce the number of costly trial-and-error experiments. Recently, we have used density functional theory (DFT) calculations with a hybrid exchange-correlation functional to accurately predict the inelastic neutron scattering (INS) phonon measurements for a model OSC system,[22] which in turn yielded an accurate prediction of μ_h. Although this effort helps establish the accuracy of hybrid functional DFT for OSCs, these calculations are extremely computationally expensive (discussed below), thus limiting system sizes to several hundred atoms for a single perfect crystalline system, only. This precludes adequate testing for system size effects, let alone the study of defect systems and new candidate OSC materials. As a result, an efficient and accurate theoretical model that is capable of optimizing current device design parameters while retaining the accuracy of higher-level quantum theories is *still lacking*.

Consequently, the goal of our current effort is to develop an efficient simulation methodology capable of accurately decoding, reproducing, and assigning the INS experimental data using only the crystal structure as an input. Purely empirical classical molecular dynamics (MD) force fields, where atomic forces are computed by parametrized potential energy surfaces, are usually highly computationally efficient but tend to yield poor results outside of their fitting regime[23] and do not allow for the simultaneous determination of electronic properties. In a recent study, we showed that MD can be used to simulate the INS spectrum of amorphous samples with some accuracy, but the large deviation of many vibrational modes from the measured spectrum makes MD insufficiently accurate to be used to simulate μ for a crystalline sample.[24] One method that circumvents these issues is to utilize a semiempirical (SE) quantum method. SE methods are based on first-principles quantum mechanics (QM) but with additional integral approximations and empirical functions based on already calculated QM results or experimental data. These modifications make SE techniques significantly more computationally efficient than standard Kohn−Sham DFT and thus can be applied to much larger system sizes and for the screening of previously unstudied OSCs. The density functional tight-binding (DFTB)[25,26] method is one such SE technique with successful applications for a number of carbon-containing materials,[27−33] including OSC molecules,[34] over a broad-range of thermodynamic conditions. DFTB uses a minimal local basis set to represent the single-electron Kohn−Sham-like eigenstates and computes the electronic states from a two-center Hamiltonian, derived directly from expansion of the Kohn−Sham Hamiltonian. DFTB is thus capable of several orders of magnitude increase in computational efficiency compared to DFT while potentially retaining much of its accuracy.[35]

One promising option for creating transferable SE models is to include additional refinements to a standard DFTB parametrization by tuning the many-body force-field known as the Chebyshev Interaction Model for Efficient Simulations (ChIMES)[36,37] to high-level DFT data. ChIMES force fields have previously been created for a number of systems, including ambient and high pressure water,[36,38] molten carbon,[37,39] and liquid carbon monoxide.[40] Recently, matching to forces[41] from DFT calculations have been shown as an efficient method for refining DFTB models,[31] including the creation of a ChIMES/DFTB model for hydrogen chemistry on δ-Pu surfaces.[42] However, these approaches have yet to be applied to systems such as OSCs, where a high degree of accuracy is needed to determine interaction energies over a wide range of energy scales (e.g., milli-electronvolt intermolecular interactions vs tenths of an electronvolt for intramolecular vibrations).

Our aim is thus to establish a methodology for the creation of highly accurate DFTB models for OSC materials that can provide an independent route to their vibrational spectra while preserving the accuracy of higher order QM methods. In this work, we demonstrate the use of a ChIMES/DFTB model that accurately computes the phonon spectrum of a model OSC system (TIPS-pentacene or TIPS-PN, discussed below) over the entire range of energy scales pertinent to these materials and validated them by comparison to a measured INS spectrum. We then show that the lower computational expense of ChIMES/DFTB enables simulation of larger supercells for better energetic convergence than the limited size scaling DFT allows. Finally, we explore the transferability of our ChIMES/DFTB model by computing the structure and vibrational spectra of four other substituted acenes (i.e., polycyclic aromatic hydrocarbons containing a rectilinear arrangement of fused benzene rings) and predict their μ_h's. We discuss the potential pathways for materials structure and property prediction that are computationally efficient and could guide synthetic experiments.

METHOD AND COMPUTATIONAL DETAILS

ChIMES Correction to DFTB Forces. The details of the ChIMES interaction model have been discussed elsewhere (e.g., refs 37 and 42), but we briefly summarize them here. The 3-body version of ChIMES is formulated by projecting the many-body interactions onto linear combinations of Chebyshev polynomials, as follows:

$$E_{\mathrm{ChIMES}} = \sum_{i}^{N}\sum_{j>i}^{N} E_{ij} + \sum_{i}^{N}\sum_{j>i}^{N}\sum_{k>j}^{N} E_{ijk} \tag{1}$$

Here, E_{ij} and E_{ijk} represent the 2-body and 3-body interaction energy, respectively, and N is the total number of atoms in the system. Specifically, they are expressed as below:

$$E_{ij} = f_P^{ij}(r_{ij}) + f_C^{ij}(r_{ij}) \sum_{n=1}^{\Theta_2} \mathfrak{c}_n^{e_i e_j} T_n(s_{ij}^{e_i e_j}) \tag{2}$$

https://dx.doi.org/10.1021/acs.jctc.0c00211
J. Chem. Theory Comput. 2020, 16, 3494−3503

In this case, $T_n(s_{ij})$ is a Chebyshev polynomial of nth order, e_i and e_j are the element types of atoms i and j, and s_{ij} is a transformation of the interatomic distance r_{ij} over the Chebyshev interval of $[-1, 1]$ (see SI for further details). In addition, Θ_2 corresponds to the 2-body polynomial order, $f_C^{ij}(r_{ij})$ is the cutoff function that forces the potential and its derivative to zero beyond a specified distance, and $f_P^{ij}(r_{ij})$ is a penalty function[36,42] that helps prevent sampling of interatomic distance below those seen in the training set. The $\mathfrak{c}_n^{e_i e_j}$ are the set of n linear polynomial coefficients for a given atom pair-type (e.g., e_i = C, e_j = Si) that are determined via a linear least-squares method from the force matching process described below. We enforce permutational invariance of the coefficients for all interactions for all six possible atom pair types in our system, e.g., $\mathfrak{c}_n^{\mathrm{SiC}} = \mathfrak{c}_n^{\mathrm{CSi}}$.

Similarly, the 3-body interaction energy function (eq 3) is expressed as a product of Chebyshev polynomials for the constituent atom pairs of a given triplet, yielding three pairs, i.e., $\binom{3}{2}$, of interactions:

$$E_{ijk} = f_C^{ij}(r_{ij}) f_C^{ij}(r_{ik}) f_C^{ij}(r_{jk}) \sum_{m=0}^{\Theta_3} \sum_{p=0}^{\Theta_3} \sum_{q=0}^{\Theta_3} {}' \mathfrak{c}_{mpq}^{e_i e_j e_k} T_m(s_{ij}^{e_i e_j}) T_p(s_{ik}^{e_i e_k}) T_q^{e_i e_k}(s_{jk}^{e_j e_k}) \tag{3}$$

The single sum in the 2-body energy function is now a triple sum over each atom pair type, with Θ_3 used to label the 3-body polynomial order and with a single permutationally invariant coefficient, $\mathfrak{c}_{mpq}^{e_i e_j e_k}$ for each 3-atom interaction for each set of triplet atom types. To guarantee that only 3-body interactions between i, j, k are counted toward the sum, only terms for which at least two of the three m, p, q indices are greater than zero are included in the 3-body energy calculation. This is denoted by the prime notation in eq 3.

The energy expression for DFTB for this work can be written as follows:

$$E_{DFTB} = E_{BS} + E_{Coul} + E_{Rep} + E_{Disp} \tag{4}$$

where E_{BS} is the band structure energy (computed via summation over occupied electronic states from the DFTB Hamiltonian), E_{Coul} is the Coulombic energy due to charge transfer (solved for self-consistently), and E_{Rep} corresponds to ion−ion repulsions, as well as Hartree and exchange-correlation double counting terms. The additional E_{Disp} term corresponds to the long-range van der Waals or dispersion energy, computed from universal force field (UFF) parameters.[43] The UFF approach has been shown to yield accurate dispersion interactions for DFTB for a number of organic systems.[32,33] For this work, we begin with the DFTB Slater-Koster parametrization known as PBC, which is typically used for solids and organic molecules containing Si.[44]

The training set to determine E_{Rep} and its forces was computed by subtracting the contributions from the band structure, Coulombic, and disperion energies from our DFT reference forces, i.e., $\vec{F}_{TRAIN} = \vec{F}_{DFT} - \vec{F}_{BS} - \vec{F}_{Coul} - \vec{F}_{Disp}$. The Chebyshev polynomial coefficients for both 2- and 3-body terms could then be solved for by minimizing the root-mean-square error (RMSE) function below:

$$\mathrm{RMSE} = \sqrt{\frac{1}{3MN} \sum_{m=1}^{M} \sum_{i=1}^{N} \sum_{\alpha=1}^{3} [F_{i_{m\alpha},\mathrm{ChIMES}} - F_{i_{m\alpha},\mathrm{TRAIN}}]^2} \tag{5}$$

In this case, we sum over the αth Cartesian component acting on atom i (N total atoms) in configuration m (M total configurations). We solve for the optimal coefficients directly, using singular value decomposition (SVD)[45] and thus bypass potentially costly nonlinear least-squares approaches.

The DFT forces for the training set trajectory were obtained from Born−Oppenheimer DFT-MD simulations using the Vienna Ab initio Software Package (VASP)[46,47] with projector augmented-wave pseudopotentials.[48] All calculations were performed with a planewave cutoff of 800 eV and the Perdew-Burke-Ernerhof (PBE) exchange-correlation functional.[49] PBE has been shown to be less accurate than hybrid functionals for INS spectra for some OSC systems.[22] Regardless, we have chosen to use PBE for our training set due to its relative computational efficiency (i.e., ease of generating training data) and in order to directly probe the accuracy of the UFF dispersion for these systems. Canonical ensemble (NVT) MD trajectories were computed at 350 K with an SCF convergence of 10^{-6}, a time step of 0.20 fs, and the Nosé−Hoover thermostat (Nosé frequency = 0.79× 10^{15} period with steps = 40.01 and mass = 0.214× 10^{-29} au).[50] We performed our MD simulations with a TIPS-PN unit cell (100 atoms in a triclinic cell) at three different densities, 0.95 g/mL, 1.0 g/mL, and 1.05 g/mL, by uniformly scaling the cell paramters, for a duration of 5 ps each in order to effectively sample the potential energies needed for our study. Uniformly spaced frames every 100 fs were then extracted from each MD simulation, producing a total of 150 configurations in the training set.

Transient Localization Theory. Charge mobility can be accurately computed through transient localization theory (TLT), which has proven to be reliable in predicting the charge carrier mobility of high performance molecular semiconductors,[51−54] given fully converged vibrational calculations. TLT is a powerful electronic framework which considers the impact of dynamic disorder (γ) and rationalizes the charge transport in high-mobility OSCs. Neither band theory or site hopping models produce accurate predictions of charge mobility or even the temperature dependence of charge mobility.[51] TLT assumes that the charge carrier diffusion is intensely restricted by coupling to thermal molecular motions (phonons). To evaluate the effect of the phonons on mobility from TLT, we compute the nonlocal electron−phonon coupling g_{ij}^I, which is an indication of how the transfer integral J_{ij} between molecules i and j is modulated by a displacement Q^I along phonon mode I. Considering a linear coupling, the nonlocal electron−phonon coupling parameters can be evaluated as numerical differentiation of the transfer integral,

$$g_{ij}^I = \left. \frac{\partial J_{ij}(\{Q^I\})}{\partial Q^I} \right|_{\{Q^I=0\}} \tag{6}$$

such that $J_{ij}(\{Q^I = 0\}) = J_{ij}$ represents the electronic coupling in the equilibrium geometry. Calculations of the transfer integrals are carried out based on ab initio methods as represented in ref 55 at the B3LYP/3-21g* level of the theory as implemented in Gaussian16.[56]

To quantify the impact of the phonons on the charge mobility at a given temperature, one can use the variance of the transfer integrals (the dynamic disorder $\gamma_{ij,T}^2$) which can be defined as follows:

https://dx.doi.org/10.1021/acs.jctc.0c00211
J. Chem. Theory Comput. 2020, 16, 3494−3503

$$\gamma_{ij,T}^2 = \frac{1}{N_k}\sum_I \frac{|g_{ij}^I|^2}{2}\coth\left(\frac{\hbar\omega_I}{2k_BT}\right) \quad (7)$$

where k_BT indicates the thermal energy, $\hbar$ is the reduced Planck constant, ω_I denotes the phonon frequency of mode I, and N_k is the number of k-points sampled in the Brillouin zone. TLT has proven to be suitable for OSC materials and bypasses the reliance on challenging time-dependent quantum simulations.[57] The effect of dynamic disorder can then be determined by a transient localization over a length L within a fluctuation time scale adjusted by the inverse of the typical intermolecular oscillation frequency ($\tau = \hbar/\omega_0$; further details in the SI). Consequently, charge mobility can be determined from the following analytical formula:

$$\mu = \frac{e}{k_BT}\frac{L^2}{2\tau} \quad (8)$$

The flowchart in Figure 1 summarizes the procedure followed to obtain the simulated INS spectra using our previously developed DFT approach (black boxes in Figure 1) and with DFTB-ChIMES (including the right loop in red boxes in Figure 1). At first glance it may appear as if ChIMES/DFTB involves more steps and has the potential to be time-consuming. However, once the training set is computed, optimal ChIMES model parameters were solved serially within ~5−10 min. In addition, the subsequent DFT-MD training trajectories for the TIPS-PN unit cell required only ~7 wall-clock hours due to the small system size and use of PBE, which was equivalent to the amount of computational time required to optimize the experimental TIPS-PN unit cell crystal structure with a hybrid functional. In our previous DFT INS calculations,[22] the rate-determining step was the single point energy and force (SPE) calculations for all the displacements to determine the vibrational density of states, which occurs after geometry optimization. To elaborate, calculation of the vibrational density of states from the TIPS-PN 2 × 2 × 1 supercell (400 atoms) required 300 symmetry-determined displacements and each displacement utilized ~990 CPU seconds with the DFT optPBE functional, whereas ChIMES/DFTB only required ~7 CPU seconds for the same calculation. Taken as a whole, the time amounted to carrying out the "extra steps" (red boxes in Flowchart 1) solving for the ChIMES parameters is negligible while the amount of computational resources saved in the SPE calculation step is substantial. As a result, performing ChIMES/DFTB in place of pure DFT for all those displacements yielded a gain in computational efficiency of approximately 3 orders of magnitude (1000×).

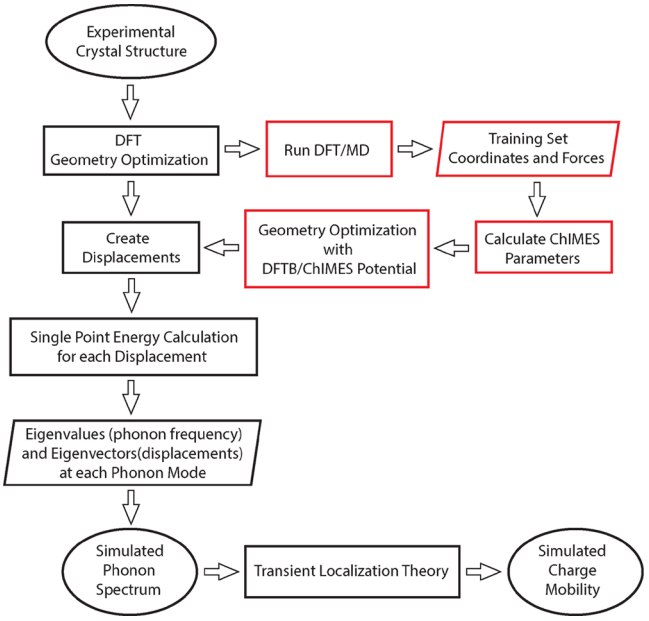

Figure 1. Flowchart of the procedure followed to compute the simulated INS spectra. The vertical flow of black boxes denotes the steps followed to calculate the simulated phonon spectrum with DFT and the horizontal loop of red boxes denotes the additional steps needed to run ChIMES/DFTB. The ChIMES/DFTB achieves computational efficiency because the single point energy calculations, which are the vast majority of the computational expense, can be performed using ChIMES/DFTB. After the phonon spectrum is simulated, TLT is used to predict μ_h.

RESULTS AND DISCUSSION

In order to determine optimal ChIMES E_{Rep} parameters, we created multiple ChIMES/DFTB models (discussed in detail in SI Section 1.1) with our training set fixed by applying different orders of the Chebyshev polynomials, starting with only 2-body interaction potentials (2B). We determined that a 2B order of 16 yielded the highest degree of accuracy with an RMSE error in the atomic forces of 5.02 kcal/(mol·Å). However, this 2B-only model yielded inaccurate peak positions and intensities in particular at frequencies of 500 cm^{-1} and below. In contrast, we found that inclusion of 3-body (3B) ChIMES interactions substantially reduced the errors, with a 2B order of 16 and 3B order of 8 yielding overall RMS errors on the atomic forces of 1.46 kcal/(mol Å). This is reflected in the correlation of the ChIMES/DFTB and DFT training forces, illustrated in Figure 2. We speculate that inclusion of 3B E_{Rep} interactions allows for improved description of rotational and bending motions of the molecular species, which in turn leads to greater improvement when compared to DFT generated spectra.

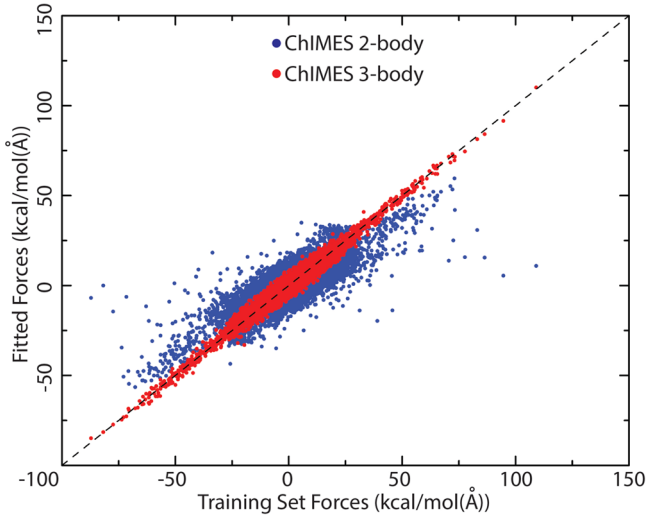

Figure 2. Correlation of the fitted forces for TIPS-PN including ChIMES 2-body only interaction potentials (in blue) and 2- and 3-body interaction potentials (in red). The dashed black line ($y = x$) is a guide to the eye, along which the data points should ideally lie.

https://dx.doi.org/10.1021/acs.jctc.0c00211
J. Chem. Theory Comput. 2020, 16, 3494−3503

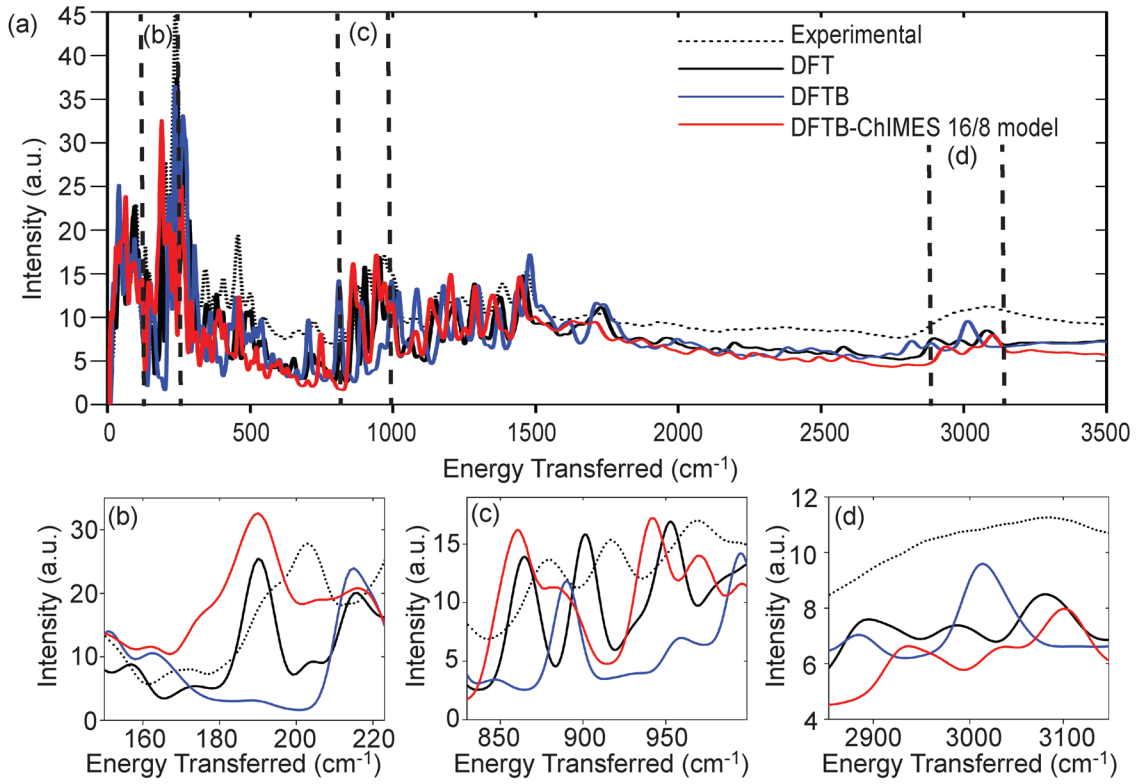

Figure 3. Experimental INS spectrum (dashed black curve) and spectra simulated with DFT (black curve), DFTB (blue curve), and ChIMES/DFTB 16/8 model (red curve) in the energy ranges (a) 10−3500 cm^{-1}, (b) 150−225 cm^{-1}, (c) 800−1000 cm^{-1}, and (d) 2800−3200 cm^{-1} for TIPS-PN.

Figure 3 shows an INS spectrum of TIPS-PN measured at the VISION spectrometer at Oak Ridge National Lab.[58,59] On the same axis we also show results from our previously published DFT/optPBE functional calculations,[22] the pbc-0-3 DFTB parametrization before tuning with ChIMES, and our optimized ChIMES/DFTB model. The computed spectra are broadened to the instrument resolution function, which masks many overlapping modes. All computed spectra have a lower baseline than the experimental INS spectrum (Figure 3) due to the presence of structural defects and finite domain sizes in the samples. In addition, the simulated peaks are slightly narrower due to an underestimation of phonon dispersion effects. To enable direct comparison to DFT, the DFTB phonon calculations were carried out using the same conditions (supercell size, cut off energy, k-point sampling mesh density, smearing width, energy convergence criteria) used in our DFT calculations.[22]

The optimized ChIMES/DFTB model (labeled 16/8) reproduced the DFT/optPBE peaks exceptionally well across the entire energy range spanning 3 orders of magnitude Figure 3. We highlight the accuracy of our model in three separate energy ranges, including intermolecular phonons (∼150−225 cm^{-1}), C−H wags (∼800−1000 cm^{-1}), and C−H stretches (∼2800−3000 cm^{-1}) (Figure 3b−d, respectively). Furthermore, the aromatic C−C−C angles undergo a bending motion around 180 cm^{-1}, and stretching motion of the C≡C bond leads to vibrational modes around 2300 cm^{-1}. The ChIMES/DFTB 16/8 model has accurately predicted some peaks that are completely missed by standard DFTB, for instance, at ∼190 cm^{-1} (Figure 3b) and 900−1000 cm^{-1} (Figure 3c). Additionally, we observe the improvement of the ChIMES/DFTB fit to DFT in Figure 3d and nearly exact prediction of the three stretch mode frequencies and intensities near 3000 cm^{-1}. Overall, we find that our ChIMES/DFTB model with UFF dispersion is able to reproduce the DFT/optPBE phonon spectrum across the full Brillouin zone using a small fraction of the computational effort.

This gain in computational efficiency allows for a system size study with our ChIMES/DFTB model that we could not perform using DFT because of computational expense. We note that ∼600 displacements were created for each TIPS-PN molecule, and DFT required ∼400 000 CPU hours of simulation time for a supercell of 2 × 2 × 1. A supercell of 2 × 2 × 2 would require ∼8× longer because DFT scales with ∼(# atoms)^3. Thus, it was not possible until using DFTB to perform a system size study. The phonon density of states (PDOS) for different supercell sizes up to 4 × 4 × 2 for TIPS-PN with ChIMES/DFTB is illustrated in Figure 4. In particular, the 1 × 1 × 1 and 2 × 2 × 1 system sizes show somewhat poor convergence, especially for peaks below 400 cm^{-1}. The charge mobility parameter μ_h is extremely sensitive to these low-lying vibrational modes.[51,60,61] Our results indicate that reasonable system-size convergence is achieved with the 2 × 2 × 2 supercell, so all further simulations were performed using a 2 × 2 × 2 supercell.

We now evaluate the transferability of our model, where we have applied our ChIMES/DFTB 16/8 model to four previously unstudied substituted acenes. TIPS-PN (Figure 5a) has a conjugated core with symmetric solubilizing side groups. We choose to model a set of four additional substituted pentacene compounds with 6,13-silylethynyl substitution but with different symmetric solublizing functional groups. Figure 5 shows the full set of molecules in this study, which are 6,13-bis (*tert*-butyldimethylsilylethynyl) pentacene

https://dx.doi.org/10.1021/acs.jctc.0c00211
J. Chem. Theory Comput. 2020, 16, 3494−3503

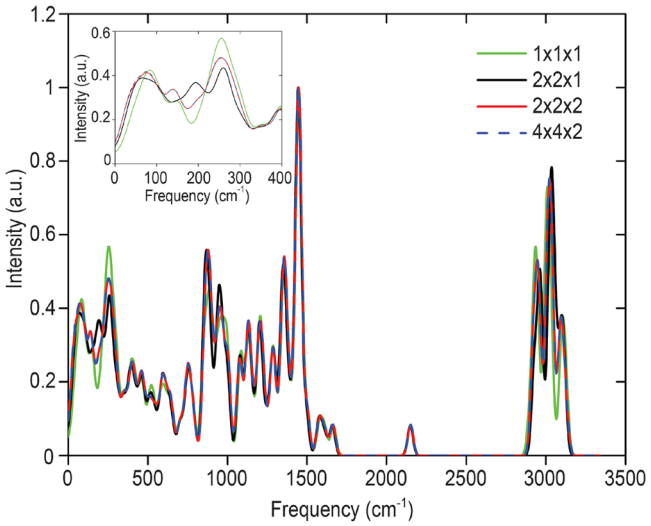

Figure 4. Normalized phonon density of states for TIPS-PN for a 1 × 1 × 1 (green curve), 2 × 2 × 1 (black curve), and 2 × 2 × 2 (red curve) and 4 × 4 × 2 supercell (dashed blue curve), with a smearing width of σ = 0.5.

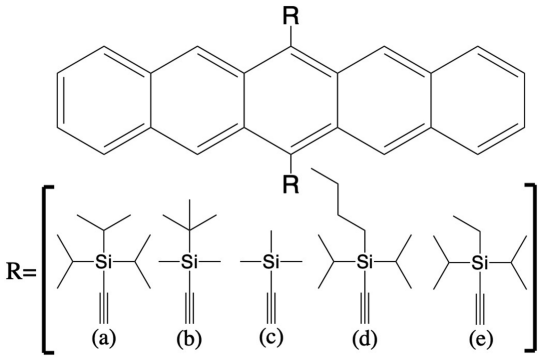

Figure 5. Chemical Structures of (a) TIPS-PN, (b) TBDMS-PN, (c) TMS-PN, (d) BDIPS-PN, and (e) EDIPS-PN.

(TBDMS-PN), 6,13-bis(trimethylsilylethynyl) pentacene (TMS-PN), 6,13-bis(butyldiisopropylsilylethynyl) pentacene (BDIPS-PN), and 6,13-bis(ethyldiisopropylsilylethynyl) pentacene (EDIPS-PN). All of these molecules have a 1-D slipped stack crystal structure. The experimental crystallographic structures for these molecules were obtained from the OCELOT (Organic Crystals in Electronic and Light-Oriented Technologies) database.[62] Structural minimization and SPE calculations for all the displacements created by Phonopy[63] were performed with ChIMES/DFTB on a 2 × 2 × 2 supercell with a Monkhorst−Pack sampling grid k-point mesh of 4 × 4 × 4. The eigenvalues and eigenvectors were then used to compute the nonlocal electron−phonon coupling parameters and μ_h for each material.

The dynamic disorder was calculated using phonons obtained from ChIMES/DFTB and TLT, as described in the Methods and Computational Details section, and was used to predict μ_h for each material. Figure 6 depicts images of each material, as well as geometry allows. The vectors labeled A, B, and C depict the three possible symmetry-allowed charge transfers from one molecule to its nearest neighbor in the high mobility plane of the crystal. TIPS-PN, TMS-PN, and TBDMS-PN only have A and B vectors marked because of negligible coupling in the C direction. The inputs for the TLT model are the transfer integrals (J_{ij}) and their standard deviation (γ_{ij}) with a single characteristic fluctuation time τ ($\hbar/\tau$ is set to 5 meV which is a typical value for molecular semiconductors as discussed in refs 22 and 57).

Computed transfer integrals, fluctuations, and hole mobilities for all the materials are reported in Table 1. Similar to other OSCs, these structures possess a high-mobility plane such that the transfer integrals between molecules out of the plane are 1 to 2 orders of magnitude smaller and therefore neglected. These results need to be approached with a careful analysis because no one feature is directly correlated with increased μ_h. In general, the hole mobility is increased by (1) minimizing the ratio of γ_i/J_i for each molecular direction, (2) increasing the total transfer integral between molecules ($J \sim J_a^2 + J_b^2 + J_c^2$), and (3) by achieving a balance between charge transfer directions. The highest predicted μ_h in this series, EDIPS-PN, was most effected by the relatively large value of J_b, the fact that there is some coupling in the C direction, and because $\gamma_i < J_i$ for all three directions. BDIPS-PN has lower total dynamic disorder and similar coupling, but because J_a and J_c are negative, the total mobility is lower. TIPS-PN has the lowest predicted mobility of this series because of low J and high γ in the B direction.

We now estimate the effect of system size on the expected value for μ_h for TIPS-PN. We want to determine whether and how the choice of system size affects the simulated μ_h. Figure 7 depicts measured and simulated μ_h for all simulated molecules. For TIPS-PN, the measured μ_h is 0.65 ± 0.35 cm^2 V^{-1} s^{-1} and is marked by a black dot with error bars.[64,65] Our previous DFT/optPBE simulation for the 2 × 2 × 1 molecular supercell size yielded a μ_h value of 1.34 cm^2 V^{-1} s^{-1}, which is larger than the measured values captured by the error bars. We recognize that, experimentally, smaller domain sizes and thus more grain boundaries will lower the experimental μ compared to computed μ based on a single crystal structure, so we

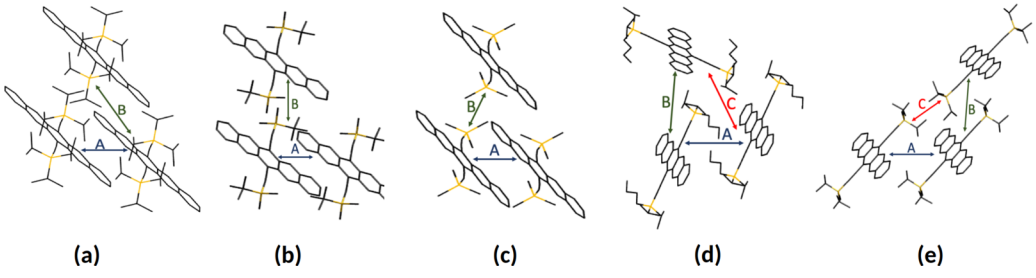

Figure 6. Graphical representation of the interacting pairs denoted as *A*, *B*, and *C* for which the transfer integrals and dynamic disorders are reported in Table 1. (a) TIPS-PN, (b) TBDMS-PN, (c) TMS-PN, (d) BDIPS-PN, and (e) EDIPS-PN.

https://dx.doi.org/10.1021/acs.jctc.0c00211
J. Chem. Theory Comput. 2020, 16, 3494−3503

Table 1. List of Materials; Transfer Integral (J) between Pairs in the High-Mobility Plane as Shown in Figure 6; Fluctuation of the Transfer Integral (γ) at 300 K; and Hole Mobility (μ_h) Computed in the Transient Localization Framework[a]

material	J_A	J_B (cm^{-1})	J_C	γ_A	γ_B (cm^{-1})	γ_C	μ_h ($cm^2\ V^{-1}\ s^{-1}$)
TIPS-PN^{DFT}	587	19.1	-	311	124	-	1.34
TIPS-PN*	587	19.1	-	381	131	-	1.15
TIPS-PN	587	19.1	-	498	143	-	0.87
TBDMS-PN	315	−19.5	-	527	12.09	-	0.97
TMS-PN	675	42.12	-	513	13.1	-	1.06
BDIPS-PN	−510	62.98	−1.5	341	18.3	0.68	1.33
EDIPS-PN	728	76	48	412	39.5	30.1	2.05

[a]Asterisk denotes the 2 × 2 × 1 supercell, whereas all others are of 2 × 2 × 2 system size. All energies were computed with ChIMES/DFTB.

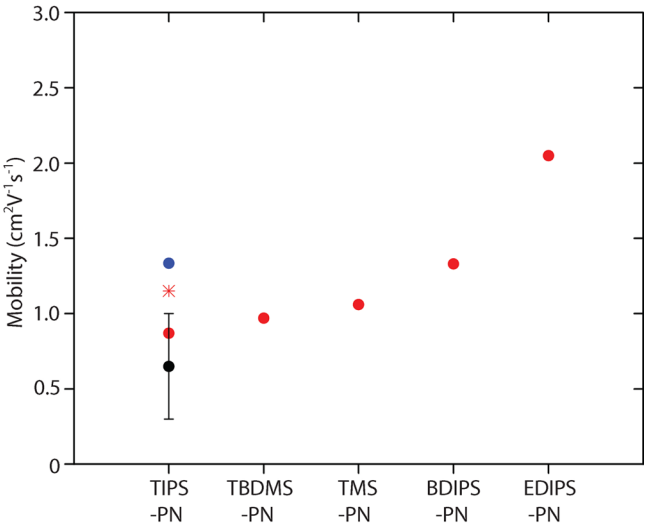

Figure 7. Illustration of the simulated hole mobilities (red dots) for all the molecules, along with TIPS-PN mobilities for experimental (black dot), DFT (blue dot), and 2 × 2 × 1 supercell (red star *).

considered 1.34 $cm^2\ V^{-1}\ s^{-1}$ to be a very good simulated estimate. In this work we developed the ChIMES/DFTB model to simulate the phonon modes. Simulation of μ_h using ChIMES/DFTB phonons yields 1.15 $cm^2\ V^{-1}\ s^{-1}$ for the 2 × 2 × 1 supercell and 0.87 $cm^2\ V^{-1}\ s^{-1}$ for the 2 × 2 × 2 supercell. Directly comparing the simulations of 2 × 2 × 1 supercells enables a direct comparison between the J's and γ's simulated from DFT vs DFTB. The J_i's, transfer integrals, are identical between the three simulations because J is calculated from the minimized structure and both DFT and DFTB simulations used the same geometry. The γ_i's, fluctuations of the transfer integral, are calculated from the simulated phonon spectrum. Comparing DFT and ChIMES/DFTB in a 2 × 2 × 1 supercell shows that the γ_i's are smaller when simulated by DFT phonons.

Comparing the two ChIMES/DFTB simulations, the μ_h for the 2 × 2 × 2 supercell is lower than for the 2 × 2 × 1 supercell. This system size dependent result shows that some low energy phonon modes are underrepresented in the 2 × 2 × 1 super cell. The system size dependence would exist using DFT simulations as well. We are confident from the scaling to a 4 × 4 × 2 supercell that a 2 × 2 × 2 supercell is sufficient to simulate the full phonon range measured using INS at VISION. Nevertheless this system size result demonstrates that a electronic simulation method with better size scaling than DFT must be used. We estimate that simulation of the phonon modes for a 2 × 2 × 2 supercell using DFT would require ∼3.2 million CPU hours, approximately our group's total annual simulation allotment at NERSC. Using ChiMES/DFTB, we performed a 2 × 2 × 2 supercell simulation that yielded almost identical phonons and predicted μ_h with several thousand CPU hours, a simulation we can perform on an in lab cluster of 128 cores in ∼1 day.

A further surprise is the ability to transfer the ChIMES/DFTB model to similar molecular structures. We only attempted to simulate substituted acenes and varied the side chain size. For all simulated acenes with side chains with <4 carbons, the ChIMES/DFTB model, optimized to TIPS-PN, nevertheless yielded a minimized structure that was identical within error to the measured crystal structure. We deemed this a sufficient proof that the ChIMES/DFTB model would also predict the dynamics correctly. However, when the number of carbons became four or greater on the side chains, the ChIMES/DFTB did not simulate the crystal structure identically to the measured one, with increasingly large deviations with longer side chains. We can conclude that the ChIMES/DFTB optimization to a single molecular structure can be transferred to similar structures with a similar ratio of SP2 to SP3 bonded carbons. Once we determined that the simulated minimized structures were sufficiently similar to the measured crystal structure, we could also predict μ_h's for four additional molecular species and we could use the data to learn why one structure will yield a higher single crystal mobility than another. While this series of simulations and μ_h predictions does not enable us to predict the properties of any arbitrary new structure, it does enable us to predict a series of similar structures that were not previously synthesized and to predict both the crystal structures and μ_h's with high accuracy. Most importantly, the simulation time and effort is lower than the synthetic time and effort, an important benchmark in materials property simulations.

CONCLUSIONS

Recent experimental and simulation results have demonstrated that charge mobility in organic semiconductors can be accurately predicted from a complete knowledge of the structure, phonon spectrum, and using transient localization theory. Our group also showed that inelastic neutron scattering data can be used to validate the phonon spectrum, but the computational cost was prohibitive. Here we demonstrate the use of DFTB force matched using a ChIMES force field to simulate the phonon spectrum with similar accuracy but ∼1000× less computational cost. The method provides an independent route to the phonon spectra of organic semiconductors and ultimately their charge mobility, while preserving the accuracy of higher order quantum methods. The fact that we have leveraged relatively efficient DFT/PBE calculations to create a DFTB model with similar accuracy to a

https://dx.doi.org/10.1021/acs.jctc.0c00211
J. Chem. Theory Comput. 2020, 16, 3494−3503

DFT hybrid functional result indicates the simplicity and some of the advantages of our approach. Electron−phonon coupling parameters computed based on the ChIMES/DFTB simulated phonon modes resulted in hole mobilities that are in quantitative agreement with available experimental data. The increased computational efficiency of ChIMES/DFTB allowed us to perform a comparison of the phonon spectra and mobility as a function of system size. We found that the phonon spectra converged for the 2 × 2 × 2 supercell, which is too large to practically simulate with DFT. Thus, the increased computational efficiency of ChIMES/DFTB enables simulations of sufficient system size. In addition, we simulated a number of different substituted acenes and demonstrated that the ChIMES/DFTB optimization to TIPS-PN is transferrable to other substituted acenes with a similar ratio of SP3 to SP2 carbons. The computational efficiency and accuracy of ChIMES/DFTB allows for a more thorough exploration of the chemical design space of OSCs and more accurate comparison with experimental efforts. Future ChIMES/DFTB modeling efforts have enormous potential as a predictive tool to help reduce costly and time-consuming trial and error experimentation to create next generation OSC materials.

■ ASSOCIATED CONTENT

Supporting Information

The Supporting Information is available free of charge at https://pubs.acs.org/doi/10.1021/acs.jctc.0c00211.

Additional details for the density functional tight binding method, materials, and transient localization theory (PDF)

■ AUTHOR INFORMATION

Corresponding Author

Adam J. Moulé − *Department of Chemical Engineering, University of California—Davis, Davis, California 95616, United States;* orcid.org/0000-0003-1354-3517; Email: amoule@ucddavis.edu

Authors

Varuni Dantanarayana − *Department of Chemistry, University of California—Davis, Davis, California 95616, United States; Lawrence Livermore National Laboratory, Livermore, California 94550, United States*

Tahereh Nematiaram − *Department of Chemistry and Materials Innovation Factory, University of Liverpool, Liverpool L69 3BX, United Kingdom;* orcid.org/0000-0002-0371-4047

Daniel Vong − *Department of Materials Science and Engineering, University of California—Davis, Davis, California 95616, United States*

John E. Anthony − *Department of Chemistry, University of Kentucky, Lexington, Kentucky 40506, United States;* orcid.org/0000-0002-8972-1888

Alessandro Troisi − *Department of Chemistry and Materials Innovation Factory, University of Liverpool, Liverpool L69 3BX, United Kingdom;* orcid.org/0000-0002-5447-5648

Kien Nguyen Cong − *Department of Physics, University of South Florida, Tampa, Florida 33620, United States*

Nir Goldman − *Department of Chemical Engineering, University of California—Davis, Davis, California 95616, United States; Lawrence Livermore National Laboratory, Livermore, California 94550, United States;* orcid.org/0000-0003-3052-2128

Roland Faller − *Department of Chemical Engineering, University of California—Davis, Davis, California 95616, United States;* orcid.org/0000-0001-9946-3846

Complete contact information is available at: https://pubs.acs.org/10.1021/acs.jctc.0c00211

Funding

This research was supported by the Department of Energy, Basic Energy Sciences, Award DE-SC0010419, including salary for V.D. and A.J.M. This research used resources of the National Energy Research Scientific Computing Center, a DOE Office of Science User Facility supported by the Office of Science of the U.S. Department of Energy under Contract No. DE-AC02-05CH11231. The INS spectrum was measured at the Spallation Neutron Source, a DOE Office of Science User Facility operated by the Oak Ridge National Laboratory, partly supported by LLNL under Contract DE-AC52-07NA27344. T.N. and A.T. acknowledge funding from ERC (Grant No. 862102).

Notes

The authors declare no competing financial interest.

■ REFERENCES

(1) Sirringhaus, H. 25th Anniversary Article: Organic Field-Effect Transistors: The Path Beyond Amorphous Silicon. *Adv. Mater.* **2014**, *26*, 1319−1335.

(2) Dou, L.; You, J.; Hong, Z.; Xu, Z.; Li, G.; Street, R. A.; Yang, Y. 25th Anniversary Article: A Decade of Organic/Polymeric Photovoltaic Research. *Adv. Mater.* **2013**, *25*, 6642−6671.

(3) Lin, P.; Yan, F. Organic Thin-Film Transistors for Chemical and Biological Sensing. *Adv. Mater.* **2012**, *24*, 34−51.

(4) Burroughes, J.; Bradley, D.; Brown, A.; Marks, R.; Mackay, K.; Friend, R.; Burns, P.; Holmes, A. Light-emitting diodes based on conjugated polymers. *Nature* **1990**, *347*, 539−541.

(5) Jou, J.-H.; Kumar, S.; Agrawal, A.; Li, T.-H.; Sahoo, S. Approaches for fabricating high efficiency organic light emitting diodes. *J. Mater. Chem. C* **2015**, *3*, 2974−3002.

(6) Dantanarayana, V.; Huang, D. M.; Staton, J. A.; Moulé, A. J.; Faller, R. Multi-scale modeling of bulk heterojunctions for organic photovoltaic applications. *Third generation photovoltaics*; In Tech: 2012; pp 29−60.

(7) Rochester, C. W.; Mauger, S. A.; Moulé, A. J. Investigating the Morphology of Polymer/Fullerene Layers Coated Using Orthogonal Solvents. *J. Phys. Chem. C* **2012**, *116*, 7287−7292.

(8) Meredith, P.; Armin, A. Scaling of next generation solution processed organic and perovskite solar cells. *Nat. Commun.* **2018**, *9*, 5261.

(9) Liu, Y.; Chen, C.-C.; Hong, Z.; Gao, J.; Yang, Y.; Zhou, H.; Dou, L.; Li, G.; Yang, Y. Solution-processed small-molecule solar cells: breaking the 10% power conversion efficiency. *Sci. Rep.* **2013**, *3*, 3356.

(10) Patel, B. B.; Diao, Y. Multiscale assembly of solution-processed organic electronics: the critical roles of confinement, fluid flow, and interfaces. *Nanotechnology* **2018**, *29*, 044004.

(11) Kanagasekaran, T.; Shimotani, H.; Shimizu, R.; Hitosugi, T.; Tanigaki, K. A new electrode design for ambipolar injection in organic semiconductors. *Nat. Commun.* **2017**, *8*, 999.

(12) Xie, W.; McGarry, K. A.; Liu, F.; Wu, Y.; Ruden, P. P.; Douglas, C. J.; Frisbie, C. D. High-Mobility Transistors Based on Single Crystals of Isotopically Substituted Rubrene-d28. *J. Phys. Chem. C* **2013**, *117*, 11522−11529.

(13) Sundar, V. C.; Zaumseil, J.; Podzorov, V.; Menard, E.; Willett, R. L.; Someya, T.; Gershenson, M. E.; Rogers, J. A. Elastomeric Transistor Stamps: Reversible Probing of Charge Transport in Organic Crystals. *Science* **2004**, *303*, 1644−1646.

(14) Podzorov, V.; Menard, E.; Borissov, A.; Kiryukhin, V.; Rogers, J. A.; Gershenson, M. E. Intrinsic Charge Transport on the Surface of Organic Semiconductors. *Phys. Rev. Lett.* **2004**, *93*, 086602.
(15) Nan, G.; Shi, Q.; Shuai, Z.; Li, Z. Influences of molecular packing on the charge mobility of organic semiconductors: From quantum charge transfer rate theory beyond the first-order perturbation. *Phys. Chem. Chem. Phys.* **2011**, *13*, 9736−46.
(16) Dantanarayana, V.; Fuzell, J.; Nai, D.; Jacobs, I. E.; Yan, H.; Faller, R.; Larsen, D.; Moule, A. J. Put Your Backbone into It: Excited-State Structural Relaxation of PffBT4T-2DT Conducting Polymer in Solution. *J. Phys. Chem. C* **2018**, *122*, 7020−7026.
(17) Heck, A.; Kranz, J. J.; Kubař, T.; Elstner, M. Multi-Scale Approach to Non-Adiabatic Charge Transport in High-Mobility Organic Semiconductors. *J. Chem. Theory Comput.* **2015**, *11*, 5068−5082.
(18) Eggeman, A. S.; Illig, S.; Troisi, A.; Sirringhaus, H.; Midgley, P. A. Measurement of molecular motion in organic semiconductors by thermal diffuse electron scattering. *Nat. Mater.* **2013**, *12*, 1045.
(19) Illig, S.; Eggeman, A. S.; Troisi, A.; Jiang, L.; Warwick, C.; Nikolka, M.; Schweicher, G.; Yeates, S. G.; Henri Geerts, Y.; Anthony, J. E.; Sirringhaus, H. Reducing dynamic disorder in small-molecule organic semiconductors by suppressing large-amplitude thermal motions. *Nat. Commun.* **2016**, *7*, 10736.
(20) Troisi, A.; Orlandi, G. Charge-transport regime of crystalline organic semiconductors: Diffusion limited by thermal off-diagonal electronic disorder. *Phys. Rev. Lett.* **2006**, *96*, 086601.
(21) Picon, J.-D.; Bussac, M. N.; Zuppiroli, L. Quantum Coherence and Carriers Mobility in Organic Semiconductors. *Phys. Rev. B: Condens. Matter Mater. Phys.* **2007**, *75*, 235106.
(22) Harrelson, T. F.; Dantanarayana, V.; Xie, X.; Koshnick, C.; Nai, D.; Fair, R.; Nuñez, S. A.; Thomas, A. K.; Murrey, T. L.; Hickner, M. A.; Grey, J. K.; Anthony, J. E.; Gomez, E. D.; Troisi, A.; Faller, R.; Moulé, A. J. Direct probe of the nuclear modes limiting charge mobility in molecular semiconductors. *Mater. Horiz.* **2019**, *6*, 182−191.
(23) Qi, T.; Bauschlicher, C. W.; Lawson, J. W.; Desai, T. G.; Reed, E. J. Comparison of ReaxFF, DFTB, and DFT for phenolic pyrolysis. 1. Molecular dynamics simulations. *J. Phys. Chem. A* **2013**, *117*, 11115−11125.
(24) Harrelson, T. F.; Dettmann, M.; Scherer, C.; Andrienko, D.; Moulé, A. J.; Faller, R. Computing INS spectra from molecular dynamics trajectories. **2020**, submitted.
(25) Elstner, M.; Porezag, D.; Jungnickel, G.; Elsner, J.; Frauenheim, Th.; Suhai, S.; Seifert, G.; Haugk, M. Self consistent charge density functional tight binding method for simulations of complex materials properties. *Phys. Rev. B: Condens. Matter Mater. Phys.* **1998**, *58*, 7260−7268.
(26) Aradi, B.; Hourahine, B.; Frauenheim, T. DFTB+, a sparse matrix-based implementation of the DFTB method. *J. Phys. Chem. A* **2007**, *111*, 5678.
(27) Köhler, C.; Seifert, G.; Frauenheim, T. Density functional based calculations for Fen ($n \leq 32$). *Chem. Phys.* **2005**, *309*, 23−31.
(28) Koskinen, P.; Häkkinen, H.; Seifert, G.; Sanna, S.; Frauenheim, T.; Moseler, M. Density-functional based tight-binding study of small gold clusters. *New J. Phys.* **2006**, *8*, 9.
(29) Goldman, N.; Fried, L. E. Extending the Density Functional Tight Binding Method to Carbon Under Extreme Conditions. *J. Phys. Chem. C* **2012**, *116*, 2198−2204.
(30) Cannella, C.; Goldman, N. Carbyne fiber synthesis within evaporating metallic liquid carbon. *J. Phys. Chem. C* **2015**, *119*, 21605−21611.
(31) Goldman, N.; Koziol, L.; Fried, L. E. Using force-matched potentials to improve the accuracy of density functional tight binding for reactive conditions. *J. Chem. Theory Comput.* **2015**, *11*, 4530−4535.
(32) Kroonblawd, M. P.; Pietrucci, F.; Saitta, A. M.; Goldman, N. Generating Converged Accurate Free Energy Surfaces for Chemical Reactions with a Force-Matched Semiempirical Model. *J. Chem. Theory Comput.* **2018**, *14*, 2207−2218.
(33) Kroonblawd, M. P.; Lindsey, R. K.; Goldman, N. Synthesis of Nitrogen-Containing Polycyclic Aromatic Hydrocarbons in Impacting Glycine Solutions. *Chemical Science* **2019**, *10*, 6091−6098.
(34) Niehaus, T.; Rohlfing, M.; Della Sala, F.; Di Carlo, A.; Frauenheim, Th. Quasiparticle Energies for Large Molecules: A Tight-Binding-Based Green's-Function Approach. *Phys. Rev. A: At., Mol., Opt. Phys.* **2005**, *71*, 022508.
(35) Zheng, G.; Witek, H. A.; Bobadova-Parvanova, P.; Irle, S.; Musaev, D. G.; Prabhakar, R.; Morokuma, K.; Lundberg, M.; Elstner, M.; Köhler, C.; Frauenheim, T. Parameter Calibration of Transition-Metal Elements for the Spin-Polarized Self-Consistent-Charge Density-Functional Tight-Binding (DFTB) Method: Sc, Ti, Fe, Co, and Ni. *J. Chem. Theory Comput.* **2007**, *3*, 1349.
(36) Koziol, L.; Fried, L. E.; Goldman, N. Using Force Matching To Determine Reactive Force Fields for Water under Extreme Thermodynamic Conditions. *J. Chem. Theory Comput.* **2017**, *13*, 135−146.
(37) Lindsey, R. K.; Fried, L. E.; Goldman, N. ChIMES: AForce Matched Potential with Explicit Three-Body Interactions for Molten Carbon. *J. Chem. Theory Comput.* **2017**, *13*, 6222−6229.
(38) Lindsey, R. K.; Fried, L. E.; Goldman, N. Application of the ChIMES Force Field to Nonreactive Molecular Systems: Water at Ambient Conditions. *J. Chem. Theory Comput.* **2019**, *15*, 436−447.
(39) Lindsey, R. K.; Kroonblawd, M. P.; Fried, L. E.; Goldman, N. In *Computational Approaches for Chemistry Under Extreme Conditions*; Goldman, N., Ed.; Springer Nature: 2019; Chapter Force Matching Approaches to Extend Density Functional Theory to Large Time and Length Scales.
(40) Armstrong, M. R.; Lindsey, R. K.; Goldman, N.; Nielsen, M. H.; Stavrou, E.; Zaug, J. M.; Fried, L. E.; Bastea, S. Ultrafast shock synthesis of nanocarbon from a liquid precursor. *Nat. Commun.* **2020**, *11* (1), 353.
(41) Ercolessi, F.; Adams, J. B. Interatomic Potentials from First-Principles Calculations: The Force-Matching Method. *Europhysics Letters(EPL)* **1994**, *26*, 583−588.
(42) Goldman, N.; Aradi, B.; Lindsey, R. K.; Fried, L. E. Development of a Multi center Density Functional Tight Binding Model for Plutonium Surface Hydriding. *J. Chem. Theory Comput.* **2018**, *14*, 2652.
(43) Rappe, A. K.; Casewit, C. J.; Colwell, K. S.; Goddard, W. A.; Skiff, W. M. UFF, a full periodic table force field for molecular mechanics and molecular dynamics simulations. *J. Am. Chem. Soc.* **1992**, *114*, 10024−10035.
(44) Bartók, A. P.; Kermode, J.; Bernstein, N.; Csányi, G. Machine Learning a General-Purpose Interatomic Potential for Silicon. *Phys. Rev. X* **2018**, *8*, 041048.
(45) Press, W. H.; Teukolsky, S. A.; Vetterling, W. T.; Flannery, B. P. *Numerical recipes: The art of scientific computing*, 3rd ed.; Cambridge University Press: 2007.
(46) Kresse, G.; Furthmüller, J. Efficiency of ab-initio total energy calculations for metals and semiconductors using a plane-wave basis set. *Comput. Mater. Sci.* **1996**, *6*, 15−50.
(47) Kresse, G.; Furthmüller, J. Efficient iterative schemes for ab initio total-energy calculations using a plane-wave basis set. *Phys. Rev. B: Condens. Matter Mater. Phys.* **1996**, *54*, 11169−11186.
(48) Kresse, G.; Joubert, D. From ultrasoft pseudopotentials to the projector augmented-wave method. *Phys. Rev. B: Condens. Matter Mater. Phys.* **1999**, *59*, 1758−1775.
(49) Perdew, J. P.; Burke, K.; Ernzerhof, M. Generalized Gradient Approximation Made Simple. *Phys. Rev. Lett.* **1996**, *77*, 3865.
(50) Evans, D. J.; Holian, B. L. The Nose−Hoover thermostat. *J. Chem. Phys.* **1985**, *83*, 4069−4074.
(51) Fratini, S.; Ciuchi, S.; Mayou, D.; de Laissardière, G. T.; Troisi, A. A map of high-mobility molecular semiconductors. *Nat. Mater.* **2017**, *16*, 998.
(52) Nematiaram, T.; Ciuchi, S.; Xie, X.; Fratini, S.; Troisi, A. Practical Computation of the Charge Mobility in Molecular Semiconductors Using Transient Localization Theory. *J. Phys. Chem. C* **2019**, *123*, 6989−6997.

https://dx.doi.org/10.1021/acs.jctc.0c00211
J. Chem. Theory Comput. 2020, 16, 3494−3503

(53) Fratini, S.; Mayou, D.; Ciuchi, S. The Transient Localization Scenario for Charge Transport in Crystalline Organic Materials. *Adv. Funct. Mater.* **2016**, *26*, 2292−2315.
(54) Fratini, S.; Ciuchi, S. Dynamical localization corrections to band transport. *Phys. Rev. Res.* **2020**, *2*, 013001.
(55) Troisi, A.; Orlandi, G. The hole transfer in DNA: calculation of electron coupling between close bases. *Chem. Phys. Lett.* **2001**, *344*, 509−518.
(56) Frisch, M. J.; Trucks, G. W.; Schlegel, H. B.; Scuseria, G. E.; Robb, M. A.; Cheeseman, J. R.; Scalmani, G.; Barone, V.; Petersson, G. A.; Nakatsuji, H.; Li, X.; Caricato, M.; Marenich, A. V.; Bloino, J.; Janesko, B. G.; Gomperts, R.; Mennucci, B.; Hratchian, H. P.; Ortiz, J. V.; Izmaylov, A. F.; Sonnenberg, J. L.; Williams-Young, D.; Ding, F.; Lipparini, F.; Egidi, F.; Goings, J.; Peng, B.; Petrone, A.; Henderson, T.; Ranasinghe, D.; Zakrzewski, V. G.; Gao, J.; Rega, N.; Zheng, G.; Liang, W.; Hada, M.; Ehara, M.; Toyota, K.; Fukuda, R.; Hasegawa, J.; Ishida, M.; Nakajima, T.; Honda, Y.; Kitao, O.; Nakai, H.; Vreven, T.; Throssell, K.; Montgomery, J. A., Jr.; Peralta, J. E.; Ogliaro, F.; Bearpark, M. J.; Heyd, J. J.; Brothers, E. N.; Kudin, K. N.; Staroverov, V. N.; Keith, T. A.; Kobayashi, R.; Normand, J.; Raghavachari, K.; Rendell, A. P.; Burant, J. C.; Iyengar, S. S.; Tomasi, J.; Cossi, M.; Millam, J. M.; Klene, M.; Adamo, C.; Cammi, R.; Ochterski, J. W.; Martin, R. L.; Morokuma, K.; Farkas, O.; Foresman, J. B.; Fox, D. J. *Gaussian16*, revision C.01; Gaussian Inc.: Wallingford CT, 2016.
(57) Nematiaram, T.; Troisi, A. Modelling Charge Transport in High-Mobility Molecular Semiconductors: Balancing Electronic Structure and Quantum Dynamics Methods with the Help of Experiments. *J. Chem. Phys.* **2020**, *152*, 190902.
(58) Seeger, P. A.; Daemen, L. L.; Larese, J. Z. Resolution of VISION, a crystal-analyzer spectrometer. *Nucl. Instrum. Methods Phys. Res., Sect. A* **2009**, *604*, 719−728.
(59) Parker, S. F.; Ramirez-Cuesta, A. J.; Daemen, L. Vibrational spectroscopy with neutrons: recent developments. *Spectrochim. Acta, Part A* **2018**, *190*, 518−523.
(60) Harrelson, T. F.; Cheng, Y. Q.; Li, J.; Jacobs, I. E.; Ramirez-Cuesta, A. J.; Faller, R.; Moulé, A. J. Identifying Atomic Scale Structure in Undoped/Doped Semicrystalline P3HT Using Inelastic Neutron Scattering. *Macromolecules* **2017**, *50*, 2424−2435.
(61) Schweicher, G.; D'Avino, G.; Ruggiero, M. T.; Harkin, D. J.; Broch, K.; Venkateshvaran, D.; Liu, G.; Richard, A.; Ruzie, C.; Armstrong, J.; Kennedy, A. R.; Shankland, K.; Takimiya, K.; Geerts, Y. H.; Zeitler, J. A.; Fratini, S.; Sirringhaus, H. Chasing the killer phonon mode for the rational design of low disorder, high mobility molecular semiconductors. *Adv. Mater.* **2019**, *31*, 1902407.
(62) 2019. https://oscar.as.uky.edu/repo/datalist.
(63) Togo, A.; Chaput, L.; Tanaka, I. Distributions of phonon lifetimes in Brillouin zones. *Phys. Rev. B: Condens. Matter Mater. Phys.* **2015**, *91*, 094306.
(64) Payne, M. M.; Parkin, S. R.; Anthony, J. E.; Kuo, C.-C.; Jackson, T. N. Organic Field-Effect Transistors from Solution-Deposited Functionalized Acenes with Mobilities as High as 1 cm2/V·s. *J. Am. Chem. Soc.* **2005**, *127*, 4986−4987.
(65) Park, S. K.; Jackson, T. N.; Anthony, J. E.; Mourey, D. A. High mobility solution processed 6,13-bis(triisopropyl-silylethynyl) pentacene organic thin film transistors. *Appl. Phys. Lett.* **2007**, *91*, 063514.

https://dx.doi.org/10.1021/acs.jctc.0c00211
J. Chem. Theory Comput. 2020, 16, 3494−3503